Minimax Theory and its Applications
Volume 11 (2026), No. 3s, 840 to 853

CS-MEAN: Cerebral Small Vessel Disease Classification via Deep Mobile Efficient Attention Network

Nandhini S[1*], Vanitha K[2]

[1,2]Department of Computer Science and Engineering, Faculty of Engineering, Karpagam Academy of Higher Education, Coimbatore, Tamil Nadu, India.
Email: nandhiniphd07@gmail.com*, profvanithacse@gmail.com

Abstract
Cerebral small vessel disease (CSVD) affects the small blood vessels, that lead to reduced blood flow, stroke, and cognitive decline. However, many existing approaches focus mainly on MRI-based classification and lack effective detection of the disease. To overcome this issue, a novel deep learning (DL)-based CS-MEAN model is proposed for CSVD classification using fundus images from RFMiD dataset. Contrast Limited Adaptive Histogram Equalization (CLAHE) with Frangi (CLAFra) filter is used to enhance the fundus image and to remove the noise in the fundus image. TransU Net contains an encoder-decoder and transformer block to accurately segment the microaneurysm region from the fundus images. The hybrid MobileNet with Efficient Attention (MobileEffi) network extracts the spatial and structural (S2) features gathered from the pre-processed and the segmented images. These S2 features are further fused and classified using the Fully Connected (FC) layer as normal or abnormal. The evaluation metrics of the proposed CS-MEAN are assessed with accuracy, precision, recall, specificity, F1-score, Dice index and Jaccard index. From the experimental analysis, the proposed CS-MEAN model attains an overall accuracy of 99.02% and F1-score of 97.23% for efficient CSVD classification. Moreover, the proposed CS-MEAN model improves the overall accuracy by 1.63%, 1.71%, 0.99%, 0.81% and 0.38% better than SVM, AutoGluon, Mask R-CNN, U-Net with cross-sequence attention, and CNN respectively.

Keywords: Cerebral small vessel disease, Fundus Image, Deep Learning, Microaneurysm, Trans-UNet

1. Introduction

Cerebral small vessel disease (CSVD) is a progressive degenerative disorder that affects small-calibres cerebral blood vessels, causing pathological changes in cerebral microarteries, small arteries, capillaries, and venules [1]. CSVD is caused by changes in small blood vessels, including endothelial dysfunction and blood-brain barrier disruption. It is also caused due to hypertension, age, inflammation, and oxidative stress are the major influences [2]. CSVD has several contributory factors, including amyloid pathology, lymphatic system malfunction, and vascular anomalies. These factors reduce waste clearance and cerebral blood flow, causing small vessel damage and cognitive impairment [3]. Cognitive impairment is a prominent symptom of CSVD, especially in memory and executive function. It focuses mostly on brain damage rather than physical symptoms [4,5].

CSVD is common in low- and middle-income countries, with white matter hyperintensities found in 20.5% of community groups, 40.5% of stroke patients, and 58.4% of dementia patients [6]. The paper used I^2 statistics to quantify heterogeneity to Low, medium, and high heterogeneity represented by 25%, 50%, and 75%, respectively with statistical significance at $p<0.05$ [7]. Cerebral Small Vessel Disease contributes to almost one-fifth of ischemic strokes and 45% of dementias. It affects small perforating arterioles that supply the brain's subcortical white matter, resulting in abnormalities on advanced neuroimaging [8].

Diagnostic tools mostly rely on magnetic resonance imaging (MRI) and ex vivo MRI-histopathology correlation. MRI is used to detect CSVD indicators such as white matter hyperintensities, microbleeds, and lacunar infarctions, while ex vivo MRI-histology validates the imaging results [9,10]. Advanced MRI diagnostic methods such as diffusion tensor imaging (DTI), susceptibility-weighted imaging (SWI), functional MRI (fMRI), arterial spin labeling (ASL), and high-resolution structural MRI are used to diagnose CSVD [11]. However, the relationship between Optical coherence tomography angiography (OCTA) based retinal microvascular changes and CSVD is not well established, limiting its applicability in early detection [12].

The development of Artificial Intelligence (AI) has produced promising results in CSVD classification [13]. Deep Learning (DL) algorithms like MobileNet [14] and Adaptive Dense Neural Network are widely used for

disease classification [15]. Machine learning (ML) algorithms like Kernel Fuzzy C-Mean and SVM demonstrated remarkable performance for feature extraction and classification [16,17]. However, most existing research focuses on MRI-based classification and large-scale vascular characteristics, with little focus on early microvascular problems. To overcome these issues, a novel CS-MEAN model is proposed with the combination of DL-based microaneurysm segmentation and S2 feature extraction with fundus image. The key contribution of the proposed CS-MEAN is listed as follows,

- The CLAFra filter is the combination of Contrast LimitedAdaptive Histogram Equalization (CLAHE) with Frangi filter to remove the noise and enhance the fundus images.
- The proposed CS-MEAN modelutilized a Transformer with UNet(Trans-UNet) for segmenting the microaneurysm region for accurate and efficient classification of CSVD.
- The hybrid Mobile Net integrate with Efficient attention (MobiEffi) Network for extracting the S^2 features by taking the input from the pre-processed and segmented images.
- TheS^2 features are fused in the fully connected layer (FC) to classify the CSVD as normal or abnormal.
- The performance of the proposed CS-MEAN model has been evaluated using Accuracy, Precision, Recall, Specificity,F1-score, DiceInde and Jaccard Index for efficient classification of CSVD.

The rest of the research was pre-arranged as follows. The literature works are defined in section 2. Section 3 describes the proposed CS-MEAN model for classifying CSVD using fundus images. The result of the proposed CS-MEAN model was analysed and validated with different metrics in section 4. The conclusion and future work are enclosed in section

Literature Survey

Several research have been conducted to classify CSVD using a range of ML and DL methodologies. Researchers investigate various model architectures, feature extraction approaches, and optimization techniques for improving classification performance. These provides a comparative review of existing methodologies that includes suggested techniques and achieved accuracies.

In 2025 Ning Wu., et al., [18] used SVM to classify CSVD from the MRI images in conjunction with retinal vascular feature extraction and statistical modeling techniques. This method is used to predict and evaluate the severity of cerebral small vascular disease using retinal fundus images and clinical data. The model performed well, with AUC values of 0.82 for severe SVD prediction, 0.81 for PSMD, 0.77 for WMH volume, and 0.80 for CP volume.

In 2025 Lin, G., et al., [19] developed a multimodal MRI-based machine learning system using the AutoGluon platform was developed to classify MCI and NCI in CSVD patients by extracting features from T1-weighted, resting-state fMRI, and diffusion tensor imaging. The model outperformed standard approaches, with an AUC of 0.926 and 88.48% accuracy in training and 0.878 and 81.93% accuracy in validation, respectively.

In 2023 Wu, R., et al., [20] suggested a DL model using Mask R-CNN for cerebral microbleeds (CMBs) detection and a multi-instance learning (MIL) network for CSVD classification was proposed based on susceptibility-weighted MRI. The CMBs and CSVD are classified using the clinical diagnosis. The model achieved an IoU of 0.523, Dice score of 0.627 and classification AUC of 0.908 with accuracy of 0.819.

In 2025 Zhao, H., et al., [21] created a DL-based automated segmentation technique employing multisequence MRI was developed to quantify CSVD biomarkers such as WMH, CMBs, lacunes, and EPVSs. The method employs a multi-output U-Net with cross-sequence attention to boost feature learning. The model demonstrated excellent segmentation performance, with Dice scores of 0.85, 0.74, 0.76, and 0.75, indicating accurate and reliable CSVD evaluation.

In 2025 Li, Y., et al., [22] introduced an AI-based technique was utilized to extract retinal microvascular parameters from fundus images in order to assess cerebral small vessel disease. The technique assesses vessel characteristics like diameter, density, and tortuosity. The results revealed considerable retinal alterations and good associations with CSVD markers (r=-0.72), supporting their efficacy as biomarkers.

In 2026 Hsieh, YZ., et al., [23] employed a DL-based Convolutional Neural Network (CNN) to detect CSVD from MRI images. The model examines brain MRI data to detect vascular occlusions, pinpoint lesion locations, and produce labeled outputs that include coordinates and severity information. It performs well in lesion detection and clinical diagnosis, although particular accuracy metrics are not explicitly disclosed.

In 2024 Xia, P., et al., [] utilized a DL-based CSVD to detect cerebral microbleeds (CMBs) via quantitative susceptibility mapping (QSM) MRI for feature extraction. The network extracts and learns susceptibility-based features to effectively identify microbleed spots in MRI images. The model demonstrated good accuracy and sensitivity, indicating effective and dependable detection capability.

From the literature review, many methods rely only on classification of CSVD based on MRI images. These models offer excellent accuracy but need advanced models and expensive resources that limits their practical application. However, many recent approaches focus only on classification of CSVD using MRI and all the approaches extract only one feature from MRI images. To overcome these issues, a novel CS-MEAN model is employed for precise classification of CSVD by segmenting microaneurysm region from the fundus images and extract S2 features for efficient CSVD classification.

Proposed CS-MEAN Methodology

In this section, a novel CS-MEAN model is introduced to detect CSVD by segmenting microaneurysms from fundus images. The Schematic representation of the proposed CS- MEAN model is illustrated in figure1.

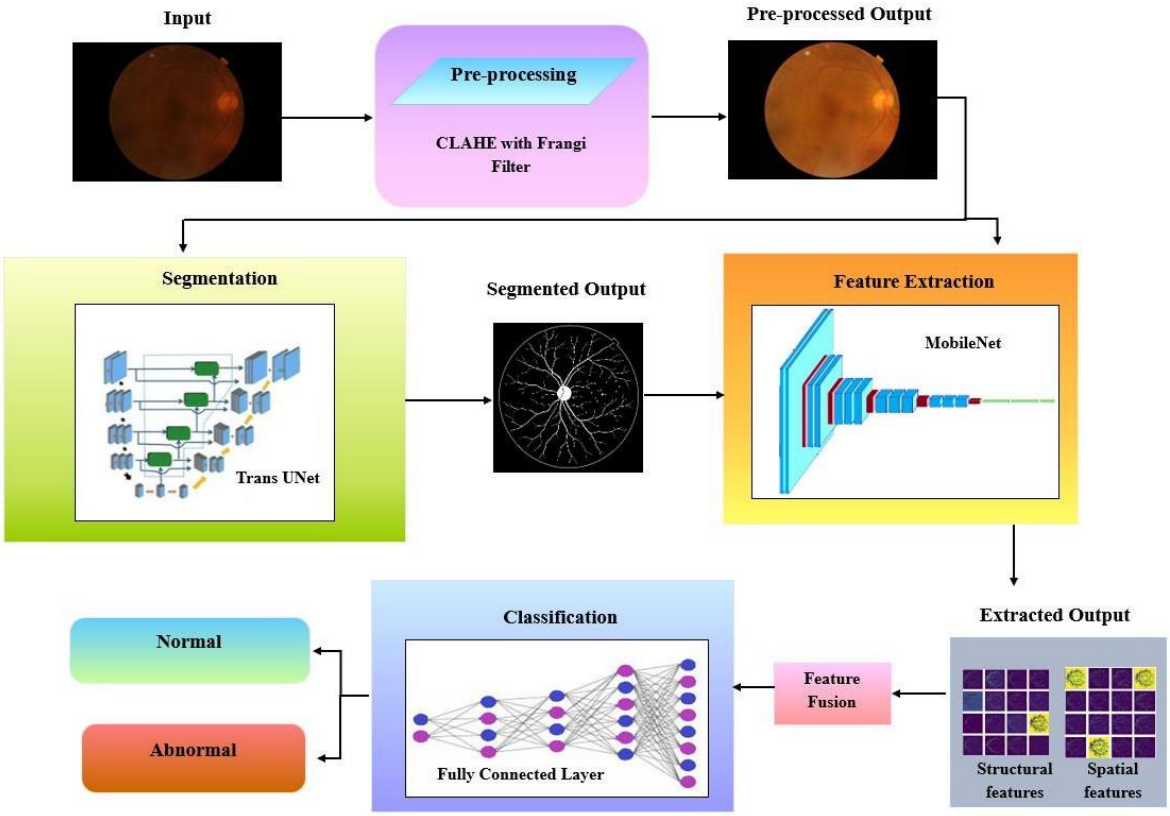


Fig. 1: Schematic representation of the proposed CS-MEAN methodology

Dataset Description

The RFMiD Dataset includes 3,200 retinal fundus images gathered for multi-disease classification tasks. It contains both normal and abnormal retinal images and covers a wide range of eye disorders, including diabetic retinopathy, glaucoma, and other retinal abnormalities. Images are typically in high-resolution format about 4288 × 2848 pixels, allowing for extensive examination of retinal architecture. The dataset is many gigabytes in size, making it ideal for training deep learning models for robust and broad retinal disease categorization.

CLAFra Filter

In the preprocessing stage, a hybrid CLAFra filter is employed with combination of Contrast LimitedAdaptive Histogram Equalization (CLAHE) and Frangi filtering is used to improve the visibility of retinal vascular and microaneurysm structures. Initially, CLAHE improves local contrast by dispersing pixel intensities while limiting over-amplification via a clipping limit defined as:

$$CLIPLIMIT=[\frac{\emptyset}{G_L}]+\beta(\emptyset-[\frac{\emptyset}{G_L}]) \quad (1)$$

Where $\emptyset$ signifies the pixel population in each block, $G_L$represents the gray level, and β represents the clip factor. To increase adaptability, a global threshold-based adjustment is introduced:

$$CLIPLIMIT=\frac{G_T}{80} \quad (2)$$

where GT is the global threshold. This update permits adaptive contrast enhancement which ensures that low-intensity regions like microaneurysms and fine vessels are adequately highlighted while avoiding artifacts. Normalization is also used to broaden the intensity range resulting in better feature representation in following processing steps.

After contrast enhancement the Frangi filter is used to highlight vessel-like structures using second-order intensity changes. The filter uses the Hessian matrix:

$$H=\begin{bmatrix} I_{aa} & I_{ab} \\ I_{ba} & I_{bb} \end{bmatrix} \quad (3)$$

WhereI_{aa},I_{ab},I_{ab},I_{bb}representtheimage'ssecond-orderpartialderivatives.Theeigenvalues are $\lambda1$ and $\lambda2$. The results of this matrix are utilized to define local structures with tubular vessel-like regions recognized based on intensity fluctuations. These are calculated as:

$$P_v=|\frac{\lambda1}{\lambda2}|, \quad R=\frac{}{\lambda_1+\lambda_2} \quad (4)$$

The vesselness response is then defined as:

$$M_\sigma=\begin{cases} 0, & \lambda2>0 \\ \exp(-\frac{P^2}{2\beta^2})(1-\exp(-\frac{R^2}{2Z^2})) & \end{cases} \quad (5)$$

To reduce sensitivity to noise Gaussian smoothing is employed before constructing the Hessian matrix.

$$G_\delta(a,b)=\frac{1}{2\pi\delta}\exp(-\frac{a^2+b^2}{2\delta^2}) \quad (6)$$

Since vessels occur at various scales multi-scale filtering is conducted and the final response is as follows:

$$M_0=\max_\delta(M(\delta)) \quad (7)$$

Finally, the Frangi-filtered output is merged with the original image to preserve structural details and improve vascular characteristics. Thus, the hybrid CLAFra filter substantially increases contrast reveals microvascular features and allows for precise segmentation of microaneurysms.

Trans-UNet

In this section, a Transformer with U-Net (Trans-UNet) is proposed to segment the microaneurysm region from the fundus images which contain an encoder-decoder and the transformer block. Initially, the pre-processed fundus image is passed through the CNN encoder to extract features. These features are then converted into patch embeddings and processed by the Transformer encoder to capture global contextual information and long-range dependencies which are essential for identifying small structures such as microaneurysms. The architecture of the Trans-UNet is shown in figure 2.

To assess the contribution of Transformer components three configurations are considered: encoder-only, decoder-only, and encoder-decoder. In the encoder-only arrangement a hybrid CNN-Transformer encoder is combined with a typical U-Net decoder to make efficient use of high-resolution feature maps. In the decoder-only arrangement a CNN encoder is followed by a Transformer-based decoder which initializes and gradually refines the embeddings P utilizing U-Net features to provide accurate segmentation maps. The encoder-decoder arrangement integrates both the Transformer encoder and decoder to improve segmentation performance.

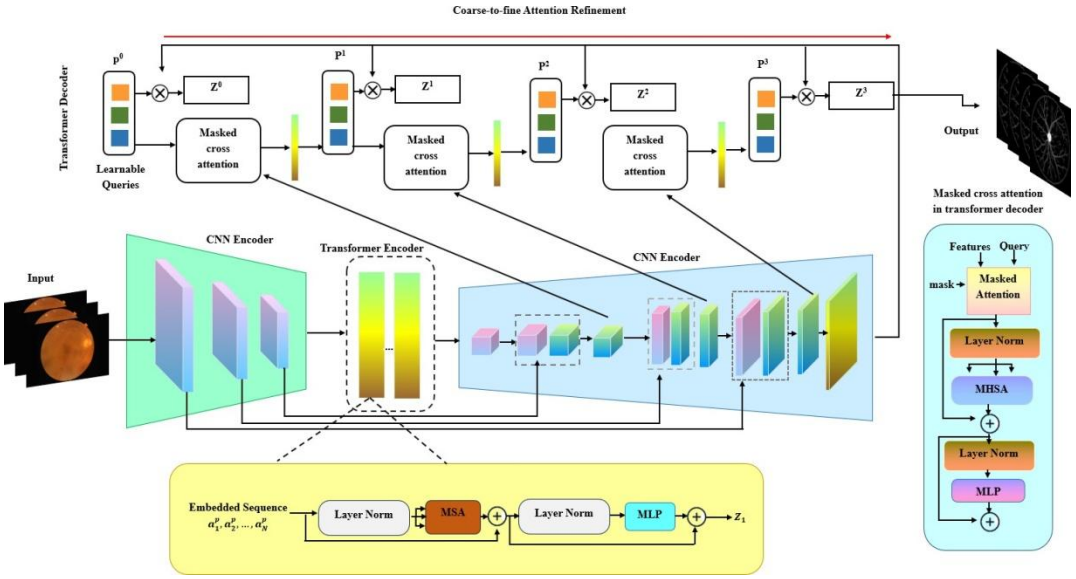


Figure 2: Architecture of the TransUNet

The model is trained with a hybrid loss function specified as follows:

$$\mathscr{L}=\lambda_0(\mathscr{L}_{CE}+\mathscr{L}_{dice})+\lambda_1\mathscr{L}_{CL} \quad (8)$$

$\mathscr{L}CE$ denotes pixel-wise cross-entropy loss, $\mathscr{L}dice$ ensures overlap accuracy between predicted and ground truth segmentation, and $\mathscr{L}CL$ reflects classification loss for candidate areas. The parameters $\lambda 0$ and $\lambda 1$ determine the balance of segmentation and classification objectives.

Furthermore, deep supervision is used at several stages of the decoder to improve training efficiency and segmentation accuracy. The TransUNet architecture effectively partitions microaneurysms by combining CNN-based spatial feature extraction with Transformer-based global context modeling, resulting in precise spatial feature maps for further feature extraction.

Feature Extraction

In this section, the proposed CS-MEAN model employs a hybrid MobileNet with Efficient Attention (MobiEffi) Network to extract the S2 features. The pre-processed image includes spatial information such as intensity, texture, and vascular patterns, whereas the segmented output highlights the specific location and structure of microaneurysms. Figure 3 illustrates the Architecture of the hybrid MobiEffi Net.

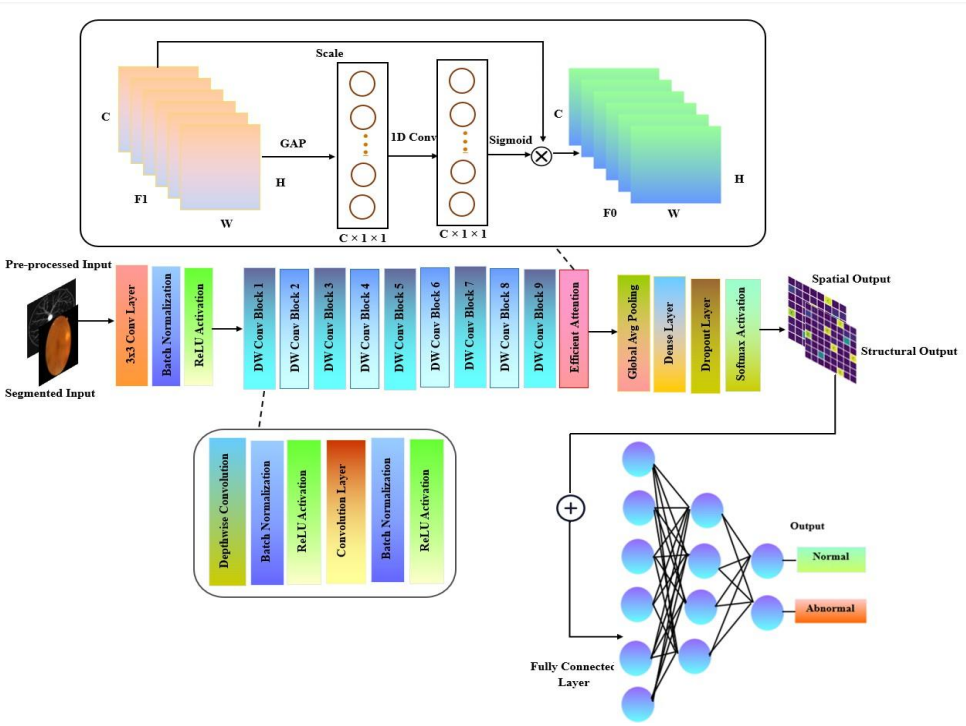


Figure 3: Architecture of hybrid MobiEffiNet

Initially, both spatial feature from the pre-processed image and structural feature from segmented image inputs are fed into the MobileNet architecture where depthwise separable convolutions extract discriminative features while being computationally efficient. These attributes are then projected into query, key, and value representations as follows:

$$Q=AW_Q, \qquad K=AW_K, \qquad V=AW_V \tag{9}$$

To improve global contextual knowledge, an attention mechanism is used. The standard self- attention is defined as follows:

$$S(Q,K,V)=softmax(\frac{QK^T}{\sqrt{D_k}})V \tag{10}$$

Due to its quadratic complexity, Efficient Attention is adopted and computed as follows:

$$G(Q,K,V)=\rho_q(Q)(\rho_k(K)^TV \tag{11}$$

where $\rho_Q$and $\rho_K$are normalization functions. This approach minimizes computing complexity while maintaining global feature interactions.

$$MultiHead(Q,K,V)=Concat(head_1,\ldots,head_h)W \tag{12}$$

$$head_u=Attention(Q_u,K_u,V_i) \tag{13}$$

In the MobiEffi Net, structural features capture texture patterns and intensity changes, while spatial features record the position and form of microaneurysms. The addition of Efficient Attention improves these representations by focusing on therapeutically significant regions while minimizing unnecessary background information. As a result, both S2 features are improved, effectively highlighting disease-specific patterns in fundus images. These complementing features are then combined to generate a unified and discriminative feature representation, hence improving the model's capacity to discern between normal and abnormal classes.

During the feature extraction stage, S2 representations are converted into feature vectors and concatenated to form a single, robust representation. This fusion feature vector integrates complementary information, which

improves overall classification performance. The integrated characteristics are then sent to a FC layer, which performs global classification operations. Similar to a multi-layer perceptron (MLP), the FC layer links neurons from preceding layers and converts the collected feature map into a flattened vector. Finally, the output layer performs classification, allowing for reliable prediction of CSVD as normal or abnormal using the global information.

Result and Discussion

The result section analyses the performance of the proposed CS-MEAN model using common metrics for CSVD classification. In this evaluation, we have analyzed several patients with their gathered fundus images between different time intervals. The experiment was conducted on a PC with Windowa-10 OS, an intel Core i9 processer, 32GB RAM, and an NVIDIA GPU with CUDA capability to speed up the DL operations. The model uses Python as the major programming language with DL frameworks such as TensorFlow and PyTorch for classifying the CSVD. The fundus images are split into 70% for training and 30% for testing the CSVD model. Figure 4 shows the experimental results of the proposed model.

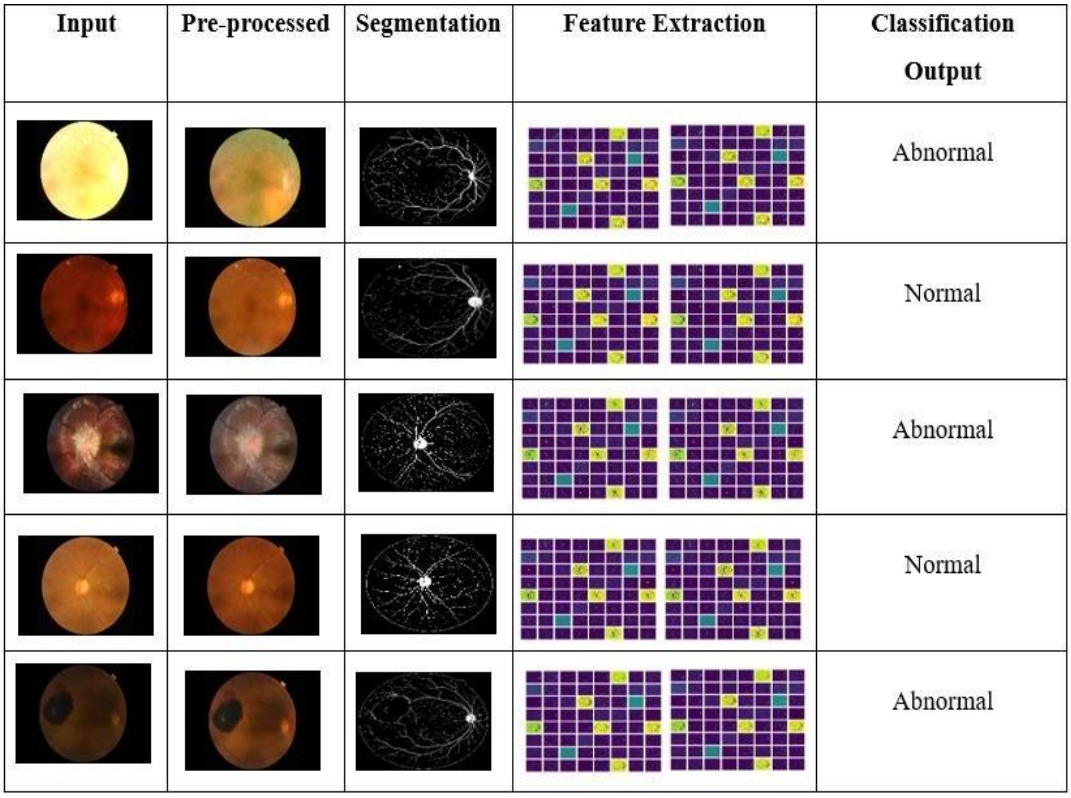


Figure 4: Experimental results of the proposed CS-MEAN model

Performance Analysis

The efficacy of the proposed CS-MEAN model performance is measured using metrics such as accuracy (AY), Precision (PN), specificity (SY), recall (RL), F1-score (F1-S), dices Index (DI) and Jaccard Index (JI). The use of CS-MEAN model for efficiently segmenting the CSVD from fundus images leads to more accurate feature extraction and classification.

$$AY = \frac{T_P+T_N}{T_P+T_N+F_P+F_N} \quad (14)$$

$$RL=\frac{T_P}{T_P+F_N} \quad (15)$$

$$PN=\frac{T_P}{T_P+F_P} \quad (16)$$

$$SY=\frac{T_N}{T_N+F_P} \quad (17)$$

$$F1-S= 2*\frac{PN\times RL}{PN+RL} \quad (18)$$

$$DI = \frac{2.T_P}{2.T_P+F_P+F_N} \quad (19)$$

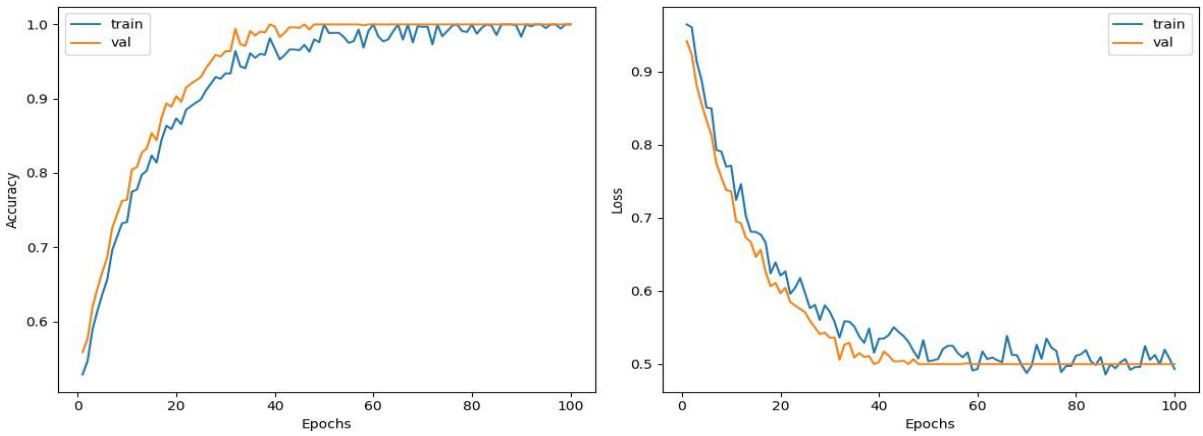
$$JI= \frac{T_P}{T_P+F_P+F_N} \quad (20)$$

From the above equation (14-20) TP represents True Positive, TN represents True Negative, FP represents False Positive, and FN denotes False Negative in the performance analysis of the CSVD classification of fundus image.

Table 1: Efficiency Analysis of the proposed CS-MEAN model

Types	AY(%)	PN(%)	SY(%)	RL (%)	F1-S(%)
Normal	98.9	98.45	97.2	97.2	97.8
Abnormal	99.14	97.89	98.32	98.32	98.05
Overall	99.02	98.17	97.76	98.54	97.23

Table 1 compares the classification performance of the CSVD using metrics like AY, PN, SY, RL and F1-S. The CS-MEAN model obtains high AY in two classes such as normal and abnormal suggesting strong classification ability. Overall, with an AY of 99.02% and F1-S of 97.23% the model is consistent and evenly performing.



(a) **(b)**

Figure 5: Training and Validation of the proposed CS-MEAN model (a) Accuracy Curve (b)Loss curve

Figure 5 depicts the training and validation performance of the proposed CS-MEAN model over 100 epochs. The accuracy graph in figure 5(a) demonstrates an increasing epoch in training and validation accuracy during

the early learning period that demonstrates effective model convergence. The precise correlation of training and validation indicates good generalization capacity with low overfitting. The loss graph in figure5(b)indicates a steady drop in both training and validation loss values as the period increases which indicates better learning efficiency. From this analysis these curves demonstrate the robustness and stability of the proposed CS-MEAN for achieving reliable CSVD classification results.

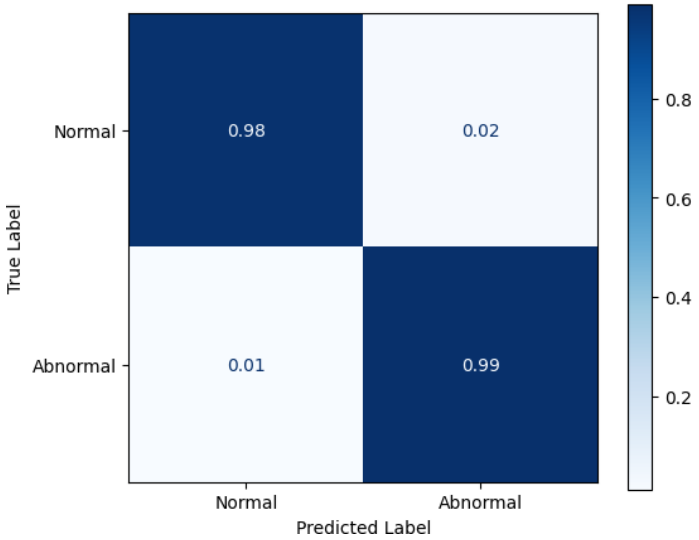


Figure 6: Confusion matrix of the proposed CS-MEAN model

Figure 6 shows the confusion matrix of the proposed CS-MEAN model for classifying the CSVD from fundus images. The model correctly classified 98% of normal samples and 99% of abnormal samples, while the misclassification rates were very low at 2% and 1%, respectively. The higher diagonal values indicate excellent prediction consistency, high sensitivity, and improved specificity, showing that the model effectively learns discriminative retinal microvascular features with minimal false predictions.

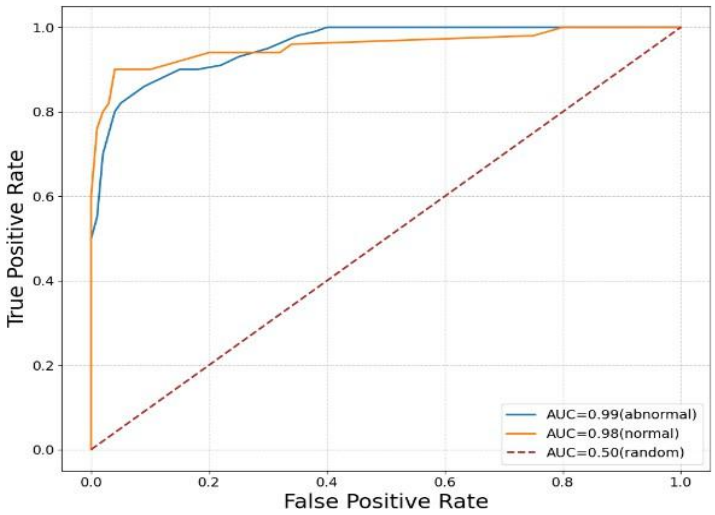


Figure 7: ROC curve of the proposed CS-MEAN model

Figure 7 shows the ROC curves for two CSVD classes evaluated with the proposed CS-MEAN classification model. The curve shows significant identification capabilities with most classes having Area Under the Curve (AUC) values greater than 0.98 that indicate consistent classification accuracy. The normal class has the lowest accuracy of 0.98 whereas abnormal class has the highest accuracy of 0.99 that indicates superior accuracy.The ROC curve closer to the top left corner indicates enhanced sensitivity and specificity across numerous classes. Overall, the results validate the capability of the proposed CS-MEAN model to effectively classify among different CSVD classes.

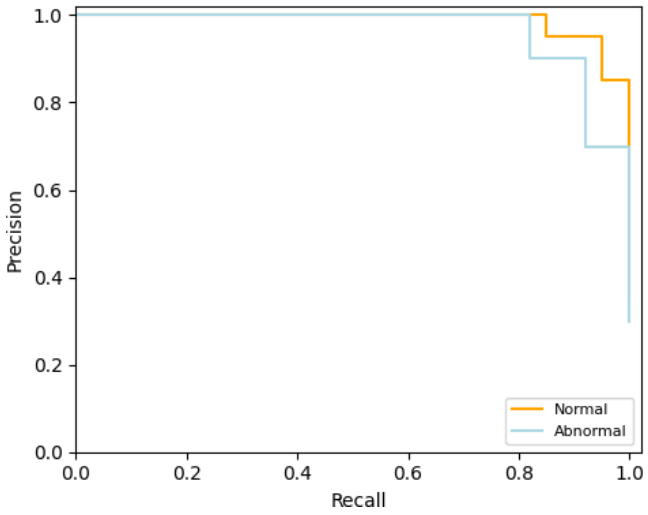


Figure 8: PR curve of the proposed CS-MEAN model

Figure 8 shows the PR curve depicts the proposed CS-MEAN model's classification performance when distinguishing between Normal and Abnormal classes. The x-axis indicates recall, which reflects the model's ability to identify all relevant samples, and the y-axis represents precision, which shows the proportion of properly predicted positive samples. The Normal class maintains a precision of 0.98 across a wide recall range, indicating that the model makes relatively few false-positive predictions while properly detecting the majority of normal samples. Similarly, the Abnormal class obtains great precision at higher recall levels, with only a tiny decrease observed near recall values of 0.99 due to an increase in false positives and false negatives. The PR curve indicates the model's excellent discriminative capabilities and robustness for accurate class-wise prediction.

Comparative Analysis

This section compares the proposed CS-MEAN model with existing models based on specific measures. The effectiveness of existing frameworks was examined in order to show that CS-MEAN model performs better in classification of CSVD. Table 2 shows the results of a comparative analysis of traditional segmentation algorithms.

Table 2: Comparison of Segmentation Networks

Network	**DI**	**JI**
UNet	0.74	0.76
SegNet	0.80	0.82
SwinUNet	0.88	0.86
TransUNet	0.97	0.94

Table 2 compares segmentation models utilizing DI and JI which measures the overlap accuracy between predicted and ground truth regions. TransUNet had the best performance of DI with 0.97 and JI with 0.94, showing superior feature representation and border localization due to long range dependencies. Overall, the findings suggest that the proposed TransU Net enhance the segmentation accuracy when compared with other Networks.

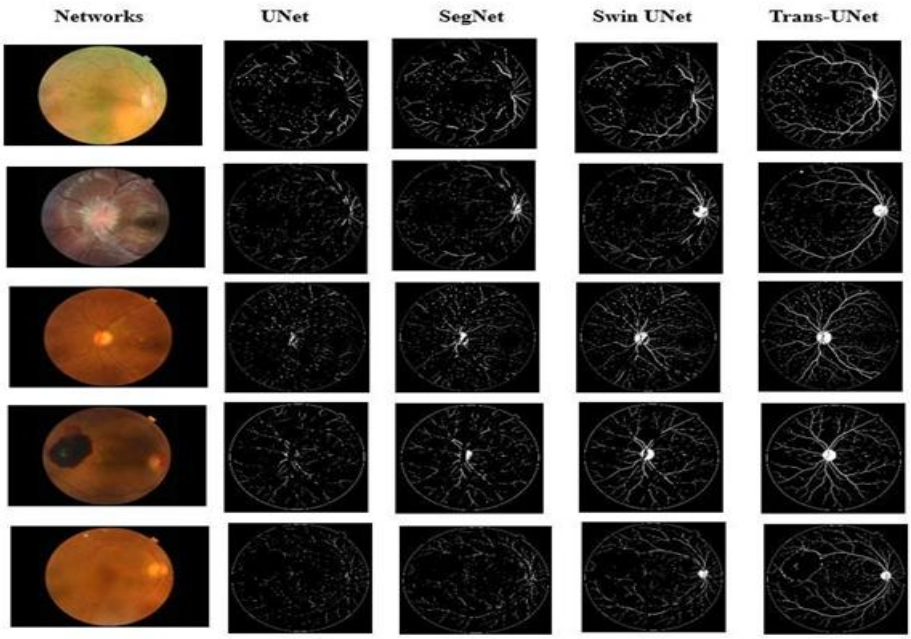


Figure 9: Segmentation comparison of the proposed CS-MEAN model

Table 3: Comparison of different DL Networks with MobiEffiNet

Network	AY (%)	PN(%)	SY(%)	RL(%)	F1-S(%)
AlexNet	98.24	97.15	96.07	97.17	95.42
ShuffleNet	98.51	97.56	96.21	97.62	96.12
SqueezeNet	98.63	98.07	96.86	98.15	96.85
DenseNet	98.89	98.11	97.64	98.27	97.01
MobiEffiNet(Ours)	99.02	98.37	97.76	98.54	97.23

Table 3 compares the effectiveness of various existing networks in extracting CSVD with the proposed model. AlexNet has lower accuracy of 98.24% because of its restricted feature extraction capability, but ShuffleNet and SqueezeNet increase accuracy by 98.51% and 98.63% through lightweight and efficient learning. DenseNet improves performance by 98.89% allowing for better feature reuse and deeper information flow. The proposed MobiEffi Net achieves the maximum accuracy of 99.02% and F1-score of 97.23% by merging MobileNet and Efficient Attention, allowing for excellent extraction of both local and global features characteristics for enhanced CSVD classification. The proposed CS-MEAN model increases the AY by 0.79%, 0.52%, 0.39%, and 0.13% over AlexNet, ShuffleNet, SqueezeNet and DenseNet respectively.

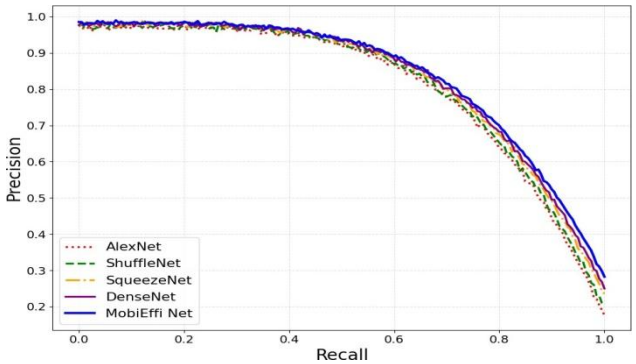


Figure 10: PR Comparison of Existing with hybrid MobiEffiNet

Figure 10 shows the PR curve of the proposed CS-MEAN model comparison with the DL Networks. The AlexNet has a precision of 0.971 and a recall of 0.9717 but its curve starts to decrease earlier due to insufficient deep feature representation. ShuffleNet enhances performance with a precision of 0.975 and recall of 0.9762 for

efficient lightweight computation, whereas SqueezeNet gets 0.980 accuracy and 0.9815 recall by improved parameter optimization and feature extraction. DenseNet achieves a precision of 0.981 and a recall of 0.9827 through dense connectivity and good feature reuse, which increases gradient propagation and contextual learning. The hybrid MobiEffi Net has the highest precision of 0.983 and recall of 0.9854, demonstrating superior discriminative capability by combining MobileNet and Efficient Attention, which improves both local and global retinal feature learning while reducing false positive predictions.

Table 4: Accuracy Comparison of Existing and Proposed CS-MEAN model

Authors	**Methods**	**Accuracy(%)**
NingWu.,etal[16]	SVM	97.41
Lin,G., etal., [17]	AutoGluon	97.86
Wu,R.,etal.,[18]	MaskR-CNN	98.03
Zhao,H.,etal.,[19]	UNet with cross-Sequence attention	98.22
Hsieh,YZ., etal.,[21]	CNN	98.64
Proposed(Ours)	CS-MEAN	99.02

In Table 4, the techniques SVM, AutoGluon, Mask R-CNN, U-Net with cross-sequence attention, and CNN are evaluated on the RFMiD dataset. The SVM model obtains 97.41% accuracy, while AutoGluon achieves 97.86%, but both are limited by inadequate feature representation, whereas Mask R-CNN achieves 98.03%, U-Net achieves 98.22%, and CNN achieves 98.64% due to enhanced localization and deep feature learning. Despite these enhancements,thesemodelsstilllackefficientintegrationof S^2features,limitingtheiroverall efficacy.Theproposed CS-MEANexceeds allotherapproaches with99.02%accuracydueto its accurate segmentation process. The proposed CS-MEAN has higher accuracy by 1.63%, 1.71%, 0.99%, 0.81% and 0.38% better than SVM, AutoGluon, Mask R-CNN, U-Net with cross-sequence attention, and CNN respectively.

Conclusion

This paper presented a novel DL-based CS-MEAN for efficient classification of cerebral small vessel disease using fundus images. The Trans-UNet is used to segment the microaneurysm region from the fundus image for efficient CSVD classification. The hybrid MobileEffi was used to extract the S2 features from the CLAFra filter and Trans-UNet for accurate classification and the Fully connected (FC) layer classify the CSVD to Normal and abnormal.

The performance of the proposed CS-MEAN model was validated with AY, PN, RL, SY, F1-S, DI and JI respectively. From the experimental result indicate that the proposed CS-MEAN model has a high classification accuracy as 99.02%, F1-Score as 97.23% DI as 0.97 and JI as 0.94 respectively. The proposed CS-MEAN model has higher accuracy by 1.63%, 1.71%, 0.99%, 0.81% and 0.38% better than SVM, AutoGluon, Mask R-CNN, U-Net with cross-sequence attention, and CNN respectively. In future, the proposed CS-MEAN model will be optimized using advanced transformer-based structures and multimodal data integration by combining fundus images with MRI and clinical data to capture more detailed disease patterns. Further enhancement can be by incorporating 3D retinal vessel analysis and adaptive feature fusion techniques for more precise CSVD classification

Reference

1. Phuah, C.L., Chen, Y., Strain, J.F., Yechoor, N., Laurido-Soto, O.J., Ances, B.M., Lee, J.M. and Alzheimer's Disease Neuroimaging Initiative, 2022. Association of data-driven white matter hyperintensity spatial signatures with distinct cerebral small vessel disease etiologies. Neurology, 99(23), pp. e2535-e2547.

2. Gao, Y., Li, D., Lin, J., Thomas, A.M., Miao, J., Chen, D., Li, S. and Chu, C., 2022. Cerebral small vessel disease: pathological mechanisms and potential therapeutic targets. Frontiers in aging neuroscience, 14, p. 961661.

3. Hong, H., Hong, L., Luo, X., Zeng, Q., Li, K., Wang, S., Jiaerken, Y., Zhang, R., Yu, X., Zhang, Y. and Lei, C., 2024. The relationship between amyloid pathology, cerebral small vessel disease, glymphatic dysfunction, and cognition: a study based on Alzheimer's disease continuum participants. Alzheimer's research & therapy, 16(1), p. 43.

4. Robert, C., Ling, L.H., Tan, E.S., Gyanwali, B., Venketasubramanian, N., Lim, S.L., Gong, L., Berboso, J.L., Richards, A.M., Chen, C. and Hilal, S., 2022. Effects of carotid artery stiffness on cerebral small-vessel disease and cognition. Journal of the American Heart Association, 11(23), p. e027295.

5. Jiang, L., Cai, X., Yao, D., Jing, J., Mei, L., Yang, Y., Li, S., Jin, A., Meng, X., Li, H. and Wei, T., 2022. Association of inflammatory markers with cerebral small vessel disease in community-based population. Journal of neuroinflammation, 19(1), p. 106.

6. Markus, H.S. and de Leeuw, F.E., 2023. Cerebral small vessel disease: recent advances and future directions. International Journal of Stroke, 18(1), pp. 4-14.

7. Yang, S. and Webb, A.J.S., 2023. Associations between neurovascular coupling and cerebral small vessel disease: A systematic review and meta-analysis. European Stroke Journal, 8(4), pp. 895-903.

8. Scheuermann, B.C., Parr, S.K., Schulze, K.M., Kunkel, O.N., Turpin, V.R.G., Liang, J. and Ade, C.J., 2023. Associations of cerebrovascular regulation and arterial stiffness with cerebral small vessel disease: a systematic review and meta-analysis. Journal of the American Heart Association, 12(23), p. e032616.

9. van Veluw, S.J., Arfanakis, K. and Schneider, J.A., 2022. Neuropathology of vascular brain health: insights from ex vivo magnetic resonance imaging–histopathology studies in cerebral small vessel disease. Stroke, 53(2), pp. 404-415.

10. Hainsworth, A.H., Markus, H.S. and Schneider, J.A., 2024. Cerebral small vessel disease, hypertension, and vascular contributions to cognitive impairment and dementia. Hypertension, 81(1), pp. 75-86.

11. Van Den Brink, H., Doubal, F.N. and Duering, M., 2023. Advanced MRI in cerebral small vessel disease. International Journal of Stroke, 18(1), pp. 28-35.

12. Fu, W., Zhou, X., Wang, M., Li, P., Hou, J., Gao, P. and Wang, J., 2022. Fundus changes evaluated by OCTA in patients with cerebral small vessel disease and their correlations: a cross-sectional study. Frontiers In Neurology, 13, p. 843198.

13. Appathurai, A., Tinu, A.S.I. and Narayanaperumal, M., 2024. MEG and PET images- based brain tumor detection using Kapur's OTSU segmentation and sooty optimized mobilenet classification. Revue Roumaine des Sciences Techniques—Série Électrotechnique Et Énergétique, 69(3), pp. 359-364.

14. Anlin Sahaya Infant Tinu, M., Appathurai, A. and Muthukumaran, N., 2024. Detection of brain tumour via reversing hexagonal feature pattern for classifying double-modal brain images. IETE Journal of Research, 70(8), pp. 7033-7043.

15. Ahilan, A., Angel Sajani, J., Jasmine Gnana Malar, A. and Muthu Kumar, B., 2023, April. Machine learning-based brain disease classification using EEG and MEG signals. In International Conference on Frontiers of Intelligent Computing: Theory and Applications (pp. 487-498). Singapore: Springer Nature Singapore.

16. Raj, J.R.F., Vijayalakshmi, K., Priya, S.K. and Appathurai, A., 2024. Brain tumor segmentation based on kernel fuzzy c-means and penguin search optimization algorithm. Signal, Image and Video Processing, 18(2), pp. 1793-1802.

17. Wang, J.L., Cheng, X.R., Meng, Z.Y. and Wang, Y.L., 2023. Impact of total cerebral small vessel disease score on ophthalmic artery morphologies and hemodynamics. Journal of Translational Medicine, 21(1), p.65.

18. Wu, N., Xu, M., Chen, S., Wu, S., Li, J., Hui, Y., Li, X., Wang, Z. and Lv, H., 2025. Retinal Vascular Morphology Reflects and Predicts Cerebral Small Vessel Disease: Evidences from Eye–Brain Imaging Analysis. Research, 8, p.0633.

19. Lin, G., Chen, W., Geng, Y., Peng, B., Liu, S., Chen, M., Pang, C., Chen, P., Lu, C., Yan, Z. and Xia, S., 2025. A multimodal MRI-based machine learning framework for classifying cognitive impairment in cerebral small vessel disease. Scientific Reports, 15(1), p.13112.

20. Wu, R., Liu, H., Li, H., Chen, L., Wei, L., Huang, X., Liu, X., Men, X., Li, X., Han, L. and Lu, Z., 2023. Deep learning based on susceptibility-weighted MR sequence for detecting cerebral microbleeds and classifying cerebral small vessel disease. BioMedical Engineering OnLine, 22(1), p.99.

21. Zhao, H., Zhang, M., Tang, W., Jin, L., Tang, J., Shi, L., Deng, X., Fu, J. and Zou, W., 2025. Deep learning-based automated segmentation for the quantitative diagnosis of cerebral small vessel disease via multisequence MRI. Frontiers in neurology, 16, p.1540923.

22. Li, Y., Zhou, X., Li, J., Zhao, Y., Yuan, Y., Yang, B., Xu, J., Wei, Q., Yan, X., Zhang, W. and Wu, Y., 2025. Deep learning assisted retinal microvasculature assessment and cerebral small vessel disease in Fabry disease. Orphanet Journal of Rare Diseases, 20(1), p.158.

23. Hsieh, Y.Z., Luo, Y.C., Pan, C., Su, M.C., Chen, C.J. and Hsieh, K.L.C., 2019. Cerebral small vessel disease biomarkers detection on MRI-sensor-based image and deep learning. Sensors, 19(11), p.2573.

24. Xia, P., Hui, E.S., Chua, B.J., Huang, F., Wang, Z., Zhang, H., Yu, H., Lau, K.K., Mak, H.K. and Cao, P., 2024. Deep-learning-based MRI microbleeds detection for cerebral small vessel disease on quantitative susceptibility mapping. Journal of Magnetic Resonance Imaging, 60(3), pp.1165-1175.